Journal of Theoretical and Applied Information Technology
15th January 2024. Vol.102. No 1

ISSN: 1992-8645 www.jatit.org E-ISSN: 1817-3195

ENERGY EFFICIENCY IN INDUSTRY 4.0: IMPLEMENTING REAL-TIME POWER FACTOR CORRECTION IN SMART MANUFACTURING

YOUSSEF ZERGUIT[1], YOUNES HAMMOUDI[2], MOSTAFA DERRHI[3]

[1,3]LTI Research Laboratory, ENSAT, Abdelmalek Essaadi University, Tangier, Morocco

[2]LAMON2E Research Laboratory, FSO, Mohammed First University, Oujda, Morocco

E-mail : [1]youssef.zerguit@etu.uae.ac.ma, [2]y.hammoudi@ump.ac.ma, [3]m.derrhi@uae.ac.ma

ABSTRACT

The Industry 4.0 paradigm has ushered in a new era of smart manufacturing, optimizing industrial processes through advanced technologies. This transformation highlights the pressing need for efficient energy utilization. Despite their crucial role in industrial power distribution, three-phase systems face persistent challenges due to load unbalances, which compromise energy efficiency and lead to suboptimal power factor levels. This unbalance results in excessive energy consumption, escalated costs, and potential equipment strain. Our research introduces an innovative methodology that harnesses Industry 4.0 technologies to reshape power factor correction and phase angle balance in three-phase systems. By strategically integrating Power Monitoring and Control Units (PMCU) within the electrical network, our approach enables real-time adjustments of capacitors and inductors. This dynamic control mechanism ensures that each load's power factor consistently approaches unity, thereby optimizing energy utilization and reducing wastage. Motivated by two key factors, our research aims to capitalize on Industry 4.0 principles for heightened adaptability and responsiveness in power systems. Moreover, the potential energy savings and operational efficiencies stemming from enhanced power factor correction have far-reaching implications for both industrial and environmental sustainability. By bridging theoretical insights with practical implementation, our work facilitates more efficient and intelligent power distribution within the Industry 4.0 landscape. In summary, our research addresses the pivotal challenge of load unbalances through an innovative methodology, contributing to the ongoing transformation of industrial processes towards enhanced efficiency, sustainability, and economic viability.

Keywords: *Automatic Balancing System, Power Factor Correction, Energy Efficiency, Three-Phase Loads, Three-Phase Balancing, Industry 4.0.*

1. INTRODUCTION

The latest development in manufacturing technologies is referred to as "Industry 4.0," which prioritizes automation and data exchange. It involves various methods such as cyber-physical systems, the Internet of Things (IoT), cloud computing, and cognitive computing [1]. The Industrial Internet of Things (IIoT) is widely recognized as one of the most important technologies that support the industrial sector. [2]. The term IIoT refers to the integration of physical and digital systems in the industrial and manufacturing sectors. It allows machines to communicate and share data in real-time, resulting in greater automation and flexibility [3].

In Industry 4.0, the concept of a smart factory is realized, where all machinery is interconnected and capable of communicating and exchanging data to achieve desired outcomes. This is possible by utilizing sensors, big data, and artificial intelligence (AI). In this framework, manufacturing is viewed as a system where physical, digital, and human components interact and collaborate in a flexible manner to achieve optimal levels of performance and productivity [4].

Industry 4.0 has the potential to bring various positive outcomes, including cost savings, increased productivity, improved product quality, and innovative commercial strategies [5].

The power factor is a metric that measures the effectiveness of electricity usage. Almost all electric energy is generated, transmitted, and distributed as alternating current. Having a low power factor is highly undesirable as it causes an increase in current, resulting in additional losses of

active power throughout the electric power supply chain [6]. This can cause an overload in the distribution system and increase the burden on the generation power plant to compensate for the expected losses [7]. Therefore, improving the power factor has immense potential to enhance energy efficiency. Addressing the issue of low power factor is crucial in achieving this goal, and power industry engineers are working actively to develop commercial and engineering methods for its correction [8].

Reactive power is a significant parameter of electrical power that causes a decrease in power factor. It is produced by two primary factors: reactive elements and unbalances in three-phase systems [9]. For instance, when an unbalanced load current and reactive power is absorbed by a single-phase load, AC rotary machines generate additional losses. Low power factor resulting from unbalanced current can adversely affect sensitive electronic equipment. Many researchers have investigated methods to minimize the additional costs associated with reactive power [10].

Unbalanced three-phase loads in industrial settings can reduce efficiency, reliability, and safety. They can cause equipment wear, power quality issues, and safety risks. To address this problem, intelligent balancing systems that utilize AI, machine learning, and the Internet of Things to monitor and control three-phase power flow have been developed. Implementing such systems can improve corporate productivity, dependability, and security. Industry 4.0 balancing systems enhance real-time monitoring, predictive maintenance, power quality, safety, and cost-effectiveness. This improves coordination and performance under various settings, making advanced technologies more robust and adaptable. Utilizing these industrial technologies may help companies achieve their Industry 4.0 ambitions [11].

To balance three-phase loads, we present an automated balancing system with power factor adjustment. Furthermore, this system is adjustable to any sort of alternating current load, whether single-phase or three-phase. Here's an overview of the remaining sections of the paper. The second part discusses the history of unbalanced systems. The third part looks into relevant literature. The fourth part concentrates on the most critical aspects of our proposed approach. The final section presents the findings and conclusions.

This study specifically investigates the application and impacts of real-time power factor correction in Industry 4.0-enabled manufacturing environments. While acknowledging the broader spectrum of Industry 4.0 applications, our research is delimited to power distribution systems within industrial settings, excluding non-industrial applications of power factor technologies.

2. BACKGROUND

2.1 Industry 4.0 and the Industrial Internet of Things (IIoT)

In 2011, a group of German economic experts introduced the term Industry 4.0 to describe the fourth industrial revolution. This revolution is being powered by several cutting-edge technologies, including the Internet of Things (IoT) [12], big data and analytics, Artificial Intelligence (AI) [13], and additive manufacturing (3D printing). These technologies are working together to revolutionize traditional factories into intelligent factories, where machines can communicate with one another and with humans, and make decisions autonomously [5].

At the core of Industry 4.0 lies the Industrial Internet of Things (IIoT), which involves the use of IoT technology in manufacturing and other industrial sectors. The IIoT facilitates real-time communication and decision-making by connecting machines, people, data, and processes [14]. This is achieved through the use of internet-connected sensors and actuators that can communicate with each other [15]. The Industrial Internet of Things (IIoT) is already revolutionizing the manufacturing industry by allowing real-time monitoring and optimization of production processes. In the future, it is expected to enable mass customization of products and the creation of new business models [2].

By implementing Industry 4.0 technologies, the manufacturing sector is anticipated to become more flexible, agile, and responsive. Additionally, these technologies are expected to enhance efficiency and productivity while decreasing costs.

2.2 Three-Phase System

In a three-phase system, current flows through three wires, and a neutral wire is used to conduct fault currents to the ground. This means that a three-phase system uses three wires for power generation, transmission, and distribution. To operate in single-phase mode, one of the three phases and the neutral wire can be extracted. The currents from the three phases add up to zero, and their phases are separated by a 120° angle (as shown in Figure 1) [16].

Journal of Theoretical and Applied Information Technology
15th January 2024. Vol.102. No 1

ISSN: 1992-8645 www.jatit.org E-ISSN: 1817-3195

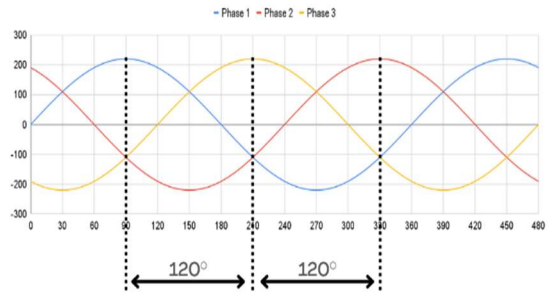

Figure 1: Waveform of a Three-Phase System.

2.3 Three-Phase Balanced and Unbalanced System/Load

A balanced three-phase system has equal magnitudes in each of its three phases, with phase angles that differ by 120 degrees from each other [17], [18]. Depending on the load, the resulting system may be either balanced or unbalanced [19]. Thus, a three-phase system is considered balanced when each of its three phases has the same impedance as the others (as shown in Figure 2-3), which can be represented as (1),(2),(3), and (4):

$$I_1 = I_{1\,peak} * sin\,(\theta) \quad (1)$$

$$I_2 = I_{2\,peak} * sin\,(\theta + \frac{2\pi}{3}) \quad (2)$$

$$I_3 = I_{3\,peak} * sin\,(\theta - \frac{2\pi}{3}) \quad (3)$$

$$I_{1\,peak} = I_{2\,peak} = I_{3\,peak} \quad (4)$$

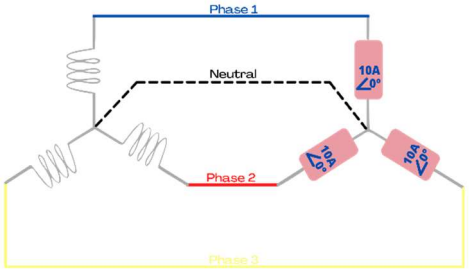

Figure 2: Balanced System.

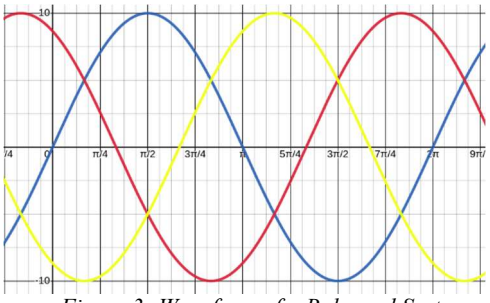

Figure 3: Waveform of a Balanced System.

Hence, an unbalanced system can be attributed to a difference in magnitude (as shown in Figure 4-5), which can be expressed using (5), (6), (7), and (8):

$$I_1 = I_{1\,peak} * sin\,(\theta) \quad (5)$$

$$I_2 = I_{2\,peak} * sin\,(\theta + \frac{2\pi}{3}) \quad (6)$$

$$I_3 = I_{3\,peak} * sin\,(\theta - \frac{2\pi}{3}) \quad (7)$$

$$I_{1\,peak} \neq I_{2\,peak} \neq I_{3\,peak} \quad (8)$$

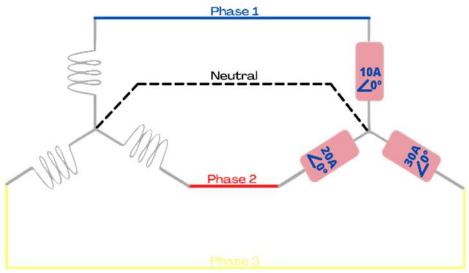

Figure 4: Magnitude Difference in an Unbalanced System.

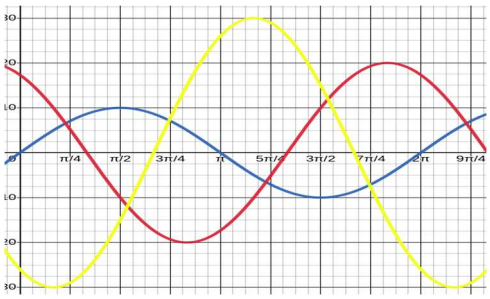

Figure 5: Waveform of an Unbalanced System Showing the Difference in Magnitude.

Alternatively, an unbalanced system may be caused by a phase difference (as shown in Figure 6-7), which can be expressed using (9), (10), (11), and (12):

$$I_1 = I_{1\,peak} * sin\,(\theta + \alpha_1) \quad (9)$$

$$I_2 = I_{2\,peak} * sin\,(\theta + \alpha_2) \quad (10)$$

$$I_3 = I_{3\,peak} * sin\,(\theta + \alpha_3) \quad (11)$$

$$I_{1\,peak} = I_{2\,peak} = I_{3\,peak} \quad (12)$$

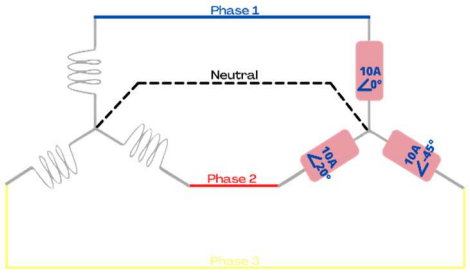

Figure 6: Phase Angle Difference in an Unbalanced System.

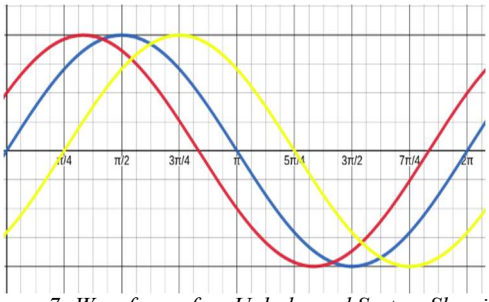

Figure 7: Waveform of an Unbalanced System Showing the Difference in Phase Angle.

3. RELATED WORKS

Ciprian Mihai Coman et al. [20] presented a paper that gives a general view of the power factor and its influence on the network operation as well as the sizing and practical realization of the proposed equipment that improves the power factor of a consumer by connecting capacitors to the power line. A new power factor correction circuit based on telemetry and remote configuration was designed and tested. The main advantage of the equipment is its remote configurability and programmability via an Internet connection, which allows easy refinement of the algorithm configuration parameters to achieve potentially better operation. The results obtained fully confirmed the theory presented and demonstrated the accuracy of the equipment design. The energy losses measured on the test equipment were reduced by 20% over a short five-day test period.

Bahaulddin Makaiber Rija et al. [21] proposed and experimentally implemented an automated single-phase power factor correction system based on the Arduino microcontroller. Their system is capable of correcting the power factor of lagging and leading loads. In addition, the system can also measure many electrical parameters of single-phase loads, such as RMS voltage, RMS current, power factor and its type, active, reactive, and apparent power. The performance of the proposed system was tested and verified by comparing the measurement results with those of a commercial digital power meter. It is found that the measurements are accurate to within 8.0% error for different load sizes with different power factors. It is also verified that the designed hardware can make the power factor of different load sizes closer to unity by connecting capacitors or inductors in parallel to the load.

Kamran Alam et al. [22] proposed a low-cost method for power factor correction on a single-phase domestic load. The proposed system continuously monitors, calculates, and corrects the power factor. The proposed system uses an Arduino-based programming environment to measure the current, voltage, power, power factor, and capacitance required to be correct. The proposed system is verified experimentally using different types of loads. With the proposed system, the power factor can be improved to a great extent and the current consumption can be reduced.

Previous research on power factor correction was limited in several ways. Firstly, it often assumed that power systems were static, when in reality they are dynamic and constantly changing as different types of loads are switched on and off. This necessitates the use of dynamic correction systems. Secondly, prior research often focused only on single-phase or balanced three-phase loads, whereas our work proposes an intelligent system for power factor correction in real-time using multi-step capacitors and inductors for each phase. This allows for power factor correction of any type of load, including dynamic and non-balanced three-phase loads.

Despite significant advancements in smart manufacturing under the Industry 4.0 paradigm, a critical challenge persists in the form of energy inefficiency due to suboptimal power factor levels in three-phase systems. This study addresses this challenge by developing and implementing a novel real-time power factor correction methodology, leveraging Industry 4.0 technologies. The research seeks to demonstrate how dynamic adjustments in power distribution can significantly enhance energy efficiency and operational sustainability in industrial contexts.

4. PROPOSED METHODOLOGY

Our approach involves the integration of a PMCU (Power Monitoring and Control Unit) before each load, which are all interconnected with the MCU (Main Control Unit) and an MPMU (Main Power Monitoring Unit) (as depicted in Figure 8). The main goal of this architecture is to enable the

Journal of Theoretical and Applied Information Technology
15th January 2024. Vol.102. No 1

ISSN: 1992-8645 www.jatit.org E-ISSN: 1817-3195

system to dynamically add or remove capacitors or inductors prior to each load, thereby achieving a power factor of 1.0 and optimizing the system's balancing configuration. This cutting-edge architecture makes use of Industry 4.0 technologies to improve cost and time efficiency, with smooth communication across devices critical for quick decision-making. To realize this, we have incorporated IIOT-based devices.

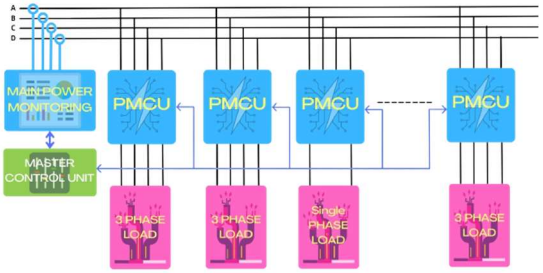

Figure 8: Schematic of Proposed Automatic Three-Phase Load Balancing System.

The PMCU (Power Monitoring and Control Unit) is an IIoT (Industrial Internet of Things) device comprised of three main components: a power monitoring unit that measures various parameters such as voltage, current, power factor, active power, reactive power, and apparent power, a power factor correction system that can adjust capacitors or inductances and a control unit that collects data from the monitoring unit, controls the capacitors and inductances and communicates with the main control unit (refer to Figure 9). Initially, an all-in-one power monitoring system (pm5100 from Schneider) was used, but its limited packet rate of one packet per 100 milliseconds was inadequate for the AC power supply frequency of 50-60 Hz, resulting in only one sample every six periods. Subsequently, a custom power monitoring board based on the ADE7785 (from Analog Devices) was created, which improved the sampling rate to one sample per period with a packet rate of one packet per 10 milliseconds. The final iteration of the device utilized an 8-channel analog-to-digital converter with a high sampling rate of 500kps (500,000 samples per second), allowing for a packet rate of one packet every 0.85 milliseconds, or 1150 samples per period. In terms of controlling the capacitors and inductances, normal relays with an operating time of 200 milliseconds were initially used, resulting in control only once every twelve periods. However, high-frequency relays with an operating time of 5 milliseconds were subsequently implemented, providing more precise control with up to four control cycles per period.

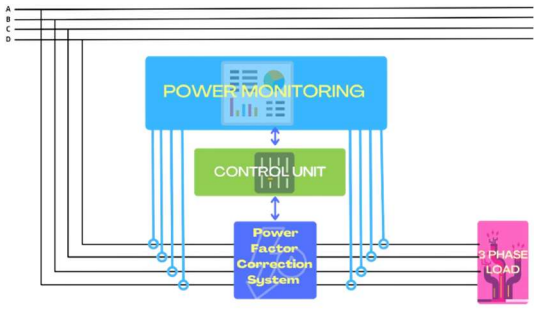

Figure 9: Schematic Diagram of Internal Components of the Power Monitoring and Control Unit.

The system operates with each PMCU acquiring data from its own PMU (power monitoring unit), which is periodically transmitted to the main control unit or upon PMCU startup. As each load is equipped with its own PMCU, it functions independently from other loads, allowing for individual adjustment of capacitor and inductor configurations. When an PMCU intends to connect a load to the power grid, it sends a request to the MCU. If the MCU possesses historical data of that PMCU, as well as current data from the MPMU and other PMCUs, it sends the appropriate configuration. In cases where no history is available, the PMCU applies a configuration based on real-time data obtained from the PMU. As configuration changes do not affect load cycles, the new configuration is implemented and data is transmitted in real-time. This ensures that a new configuration is generated each time there is a change in power factor.

We have four inputs (A, B, C, D). However, as our system is designed to independently regulate the power factor of each phase, we require a neutral detection and rerouting system. This system will only be activated when the PMCU is connected to the electrical grid, allowing the power factor correction system to be divided into two blocks (refer to Figure 10). The first block is the neutral detection and rerouting system, while the second block is the power factor correction system itself.

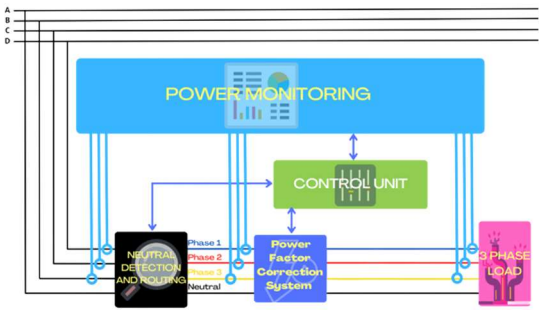

Figure 10: Schematic of Power Factor Correction System with Neutral Detection and Rerouting Block.

Journal of Theoretical and Applied Information Technology
15th January 2024. Vol.102. No 1

ISSN: 1992-8645 www.jatit.org E-ISSN: 1817-3195

In our design, the process of neutral detection and rerouting involves utilizing the data collected by the PMU and employing a combination of relays to direct the neutral to the appropriate output. Fortunately, out of the four wires in the system, three of them are phases, which means that their order is not an issue. Our goal is to ensure that only the neutral is routed to the appropriate output. We can achieve this by using six relays, as shown in Figure 11, with the configuration detailed in Table 1. The operating principle of the relay (as shown in Figure 12) is that when it is in the Off state, the output is equivalent to input 1, while when it is in the On state, the output is equivalent to input 2.

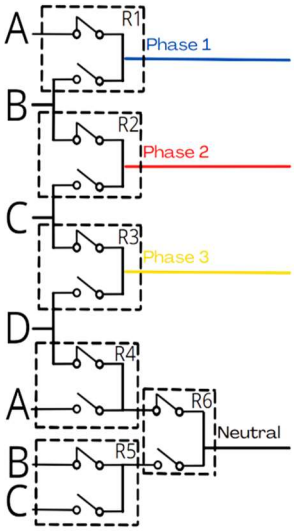

Figure 11: Schematic Diagram of the Neutral Detection and Routing System.

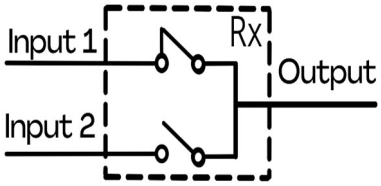

Figure 12: Schematic of a Relay.

Table 1: Possible Configuration.

Neutral	Relay 1	Relay 2	Relay 3	Relay 4	Relay 5	Relay 6
A	On	On	On	On	X	Off
B	Off	On	On	X	Off	On
C	Off	Off	On	X	On	On
D	Off	Off	Off	Off	X	Off

The previously mentioned power factor correction system can be described as a three-phase system (Figure 13), consisting of three blocks of single-phase power factor correction systems (Figure 14). Each single-phase system contains a capacitor bank and an inductor bank (Figure 15).

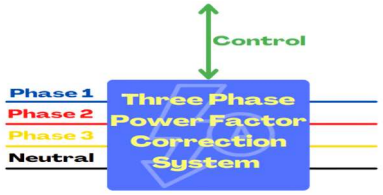

Figure 13: Schematic Diagram of a Three-Phase Power Factor Correction System.

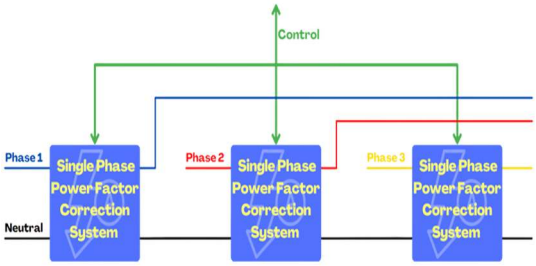

Figure 14: Schematic Diagram of Internal Components of a Three-Phase Power Factor Correction System.

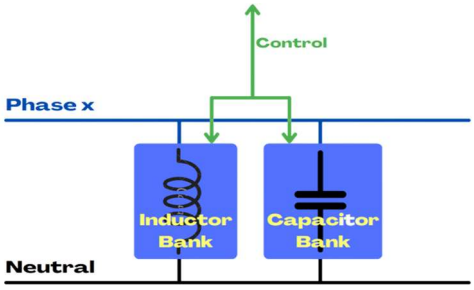

Figure 15: Schematic Diagram of Internal Components of a Single-Phase Power Factor Correction System.

To create a variable capacitance, we can use static capacitors in parallel (the capacitance values add up when they are in parallel) and add them to the network using relays (Figure 16). This gives us a variable capacitor or variable capacitor bank, where the value of the bank capacitance C_{Bank} is described as (13). In this equation, R_i represents the relay state (0 means the capacitor is not connected and 1 means it is connected), and C_i represents the value of the specific capacitor.

$$C_{Bank} = \sum_{i=0}^{n} R_i * C_i \quad (13)$$

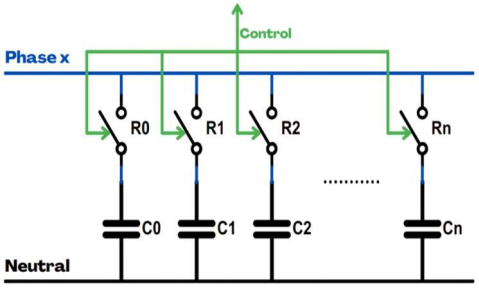

Figure 16: Schematic Diagram of a Capacitor Bank.

To create a variable inductance, we can use static inductors in series (the inductance values add up when they are in series) and add relays in parallel with each inductor. By short-circuiting the relays, we can cancel out the inductance and create a variable inductor or variable inductor bank (Figure 17). The value of the bank inductance L_{Bank} is described as (14), where R_i represents the relay state (0 means the inductor is connected and 1 means it is not connected or short-circuited), and L_i represents the value of the specific inductor. Additionally, we need a relay RL to disconnect the entire inductor bank if we want to have a null inductance and avoid short-circuiting the phase with neutral.

$$L_{Bank} = RL * (\sum_{i=0}^{n}(1 - R_i) * L_i) \quad (14)$$

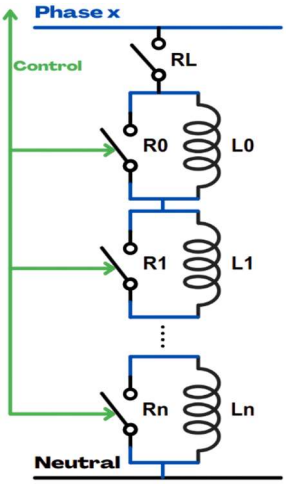

Figure 17: Schematic Diagram of an Inductor Bank.

The power factor is defined as the ratio of real power to apparent power (15). Real power is the power utilized by a load to perform work or in other words the power consumed by it. In contrast, apparent power includes both real power and reactive power, where reactive power maintains the magnetic or electric fields in the load, but it does not perform any valuable work. Real power can be calculated by multiplying the voltage and current with the cosine of the phase angle between them (16). On the other hand, apparent power is either the vector sum of real power and reactive power (17) or obtained by multiplying voltage and current (18). Based on (16) and (18), it can be concluded that the power factor is the cosine of the phase angle between current and voltage (19), which can vary from -1.0 to 1.0. The power used by a load to do real work is known as positive real power, whereas the power returned to the power source due to reactive elements in the circuit is called negative real power. In an ideal system with no reactive components, the apparent power and real power are equivalent, and the power factor is 1. Therefore, our goal is to design a system that consistently ensures a power factor of 1.0 in other words, to ensure that the reactive power is null.

$$PF = \frac{Real\ PowerP}{Apparent\ Power} = \frac{P}{S} \quad (15)$$

$$P = V * I * cos(\varphi) \quad (16)$$

$$S = \sqrt{P^2 + Q^2} \quad (17)$$

$$S = V * I \quad (18)$$

$$PF = \frac{V*I*cos(\varphi)}{V*I} = cos(\varphi) \quad (19)$$

We can use the MPU to measure the reactive power and then utilize inductors or capacitors to counteract it and achieve zero reactive power. Reactive power can either be leading or lagging. When the load is capacitive, it can store energy in an electric field and release it back into the circuit, resulting in leading reactive power (20). In this case, the current leads the voltage and the phase angle between them is negative. On the other hand, when the load is inductive, it can store energy in a magnetic field and release it back into the circuit, resulting in lagging reactive power (21). In this case, the current lags behind the voltage, and the phase angle between them is positive. Simply put, if the reactive power is negative, it means that the load is capacitive and we need to add inductance to the system to correct it. Conversely, if the reactive power is positive, it means that the load is inductive and we need to add capacitors. Once we have measured the reactive power, we must determine the required capacitance or inductance to correct it. To achieve a total reactive power of zero, we must apply reactive power that is opposite in sign to the power factor of the load (22). This can also be expressed as a function of real power and power factor (23). By using (20) and (23), we can determine the required

capacitance, as (24). Similarly, using (21) and (23), we can determine the required inductance, as (25).

$$Q_{capacitor} = -C\omega V^2 \quad (20)$$

$$Q_{inductor} = \frac{V^2}{L\omega} \quad (21)$$

$$Q_{applied} = -Q_{load} \quad (22)$$

$$Q_{applied} = -P_{load} tan\left(cos^{-1}(PF_{load})\right) \quad (23)$$

$$C = \frac{P_{load} tan\left(cos^{-1}(PF_{load})\right)}{\omega * V^2} \quad (24)$$

$$L = -\frac{V^2}{\omega * P_{load} tan\left(cos^{-1}(PF_{load})\right)} \quad (25)$$

To determine the minimum and maximum required capacitance and inductance, we computed Table 2 for capacitance using (24) and Table 3 for inductance using (25). These tables were generated by considering a real power range of 100W to 1MW and a power factor range of 0.01 to 0.99 for the capacitor case, and a power factor range of -0.99 to -0.01 for the inductor case. The results obtained from the tables indicate that the minimum capacitance required is approximately 1µF, and the maximum capacitance required is around 6.6F. Similarly, the minimum inductance required is around 1.5µH, while the maximum inductance required is approximately 10.8H. The tables were also generated to illustrate how capacitance and inductance vary in proportion to changes in real power and power factor. If we were only interested in calculating the minimum and maximum values, we could have simply used (26), (27), (28), and (29).

$$C_{min} = \frac{P_{load,min} tan\left(cos^{-1}(PF_{load,max})\right)}{\omega * V^2} \quad (26)$$

$$C_{max} = \frac{P_{load,max} tan\left(cos^{-1}(PF_{load,min})\right)}{\omega * V^2} \quad (27)$$

$$L_{min} = -\frac{V^2}{\omega * P_{load,max} tan\left(cos^{-1}(PF_{load,max})\right)} \quad (28)$$

$$L_{max} = -\frac{V^2}{\omega * P_{load,min} tan\left(cos^{-1}(PF_{load,min})\right)} \quad (29)$$

Table 2: Required Capacity Based on Real Power and Power Factor.

P(W)/PF	0.01	0.1	0.5	0.9	0.99
100	657.63	65.44	11.39	3.19	0.94
1000	6576.32	654.37	113.91	31.85	9.37
10000	65763.22	6543.68	1139.11	318.52	93.71
100000	657632.17	65436.85	11391.09	3185.22	937.12
1000000	6576321.70	654368.47	113910.93	31852.17	9371.22

Table 3: Required Inductance Based on Real Power and Power Factor.

P(W)/PF	-0.99	-0.9	-0.5	-0.1	-0.01
100	10811952.91	3180981.90	889477.28	154838.12	15406.97
1000	1081195.29	318098.19	88947.73	15483.81	1540.70
10000	108119.53	31809.82	8894.77	1548.38	154.07
100000	10811.95	3180.98	889.48	154.84	15.41
1000000	1081.20	318.10	88.95	15.48	1.54

To achieve every capacitance or inductance value within its appropriate range, it is necessary to use the minimum value of the component as the base. However, this theoretical approach is not practical in real-world scenarios. For instance, to achieve 6.6F capacitance by using a base value of 1µF, we would need 6.6 million capacitors in parallel. Similarly, to achieve 10.8H inductance using a base value of 1.5µH, we would need 7.2 million inductors in series. We can optimize the design since capacitor banks and inductor banks use relays, which have binary states of either 0 or 1. We can treat each relay as a bit, and instead of duplicating a single component value, we can use the minimum value and multiply it by 2 to the power of n. This approach is illustrated in (30) and (31), where C_i and L_i represent the desired capacitance and inductance, respectively, and i is the bit index.

$$C_i = C_{min} * 2^i \quad (30)$$

$$L_i = L_{min} * 2^i \quad (31)$$

We can calculate the number of capacitors, N_c, required when (30) equals the maximum capacity, as shown in (32). Similarly, we can calculate the number of inductors, N_L, required when (31) equals the maximum inductance, as shown in

(33). We can develop these equations further into (34) and (35), respectively. By applying a logarithmic transformation, we can obtain (36) and (37), respectively. Using (26), (27), and (36), we can derive (38). Similarly, using (28), (29), and (37), we can derive (39). As N_c and N_L are real components, we may need to round up their results if necessary.

$$C_{N_C} = C_{max} \quad (32)$$

$$L_{N_L} = L_{max} \quad (33)$$

$$C_{min} * 2^{N_C} = C_{max} \quad (34)$$

$$L_{min} * 2^{N_L} = L_{max} \quad (35)$$

$$N_C = log_2\left(\frac{C_{max}}{C_{min}}\right) \quad (36)$$

$$N_L = log_2\left(\frac{L_{max}}{L_{min}}\right) \quad (37)$$

$$N_C = log_2\left(\frac{P_{load,max}tan\left(cos^{-1}(PF_{load,min})\right)}{P_{load,min}tan\left(cos^{-1}(PF_{load,max})\right)}\right) \quad (38)$$

$$N_L = log_2\left(\frac{P_{load,max}tan\left(cos^{-1}(PF_{load,max})\right)}{P_{load,min}tan\left(cos^{-1}(PF_{load,min})\right)}\right) \quad (39)$$

In our situation, the number of capacitors (N_c) and inductors (N_L) both equal 23 components. The capacitance range is from 0 to $C_{min} * (2^{23} - 1) = 7.86\boldsymbol{F}$ with a step of C_{min}, and similarly, the inductance range is from 0 to $L_{min} * (2^{23} - 1) = 12.92\boldsymbol{H}$ with a step of L_{min}.

In order to determine which capacitors or inductors to use to achieve the desired capacitance value for the capacitor bank C_{Bank} or inductance value for the inductor bank L_{Bank}, we can utilize a combination of (13), (24), and (30) to obtain (40) for the capacitors, and (14), (25), and (31) to get (41) for the inductors (as we aim to achieve a specific inductance value, RL is set to 1). These equations can be simplified further into (42) and (43), which involve a straightforward conversion from decimal to binary (44). The output of (42) and (43) are real numbers, and therefore, they need to be rounded off before applying the decimal-to-binary conversion. In the capacitor equation, the binary state b_i is equivalent to the relay state R_i, while for the inductor equation, the binary state b_i is the inverse of the relay state R_i.

$$\sum_{i=0}^{N_C} R_i * C_{min} * 2^i = \frac{P_{load}tan\left(cos^{-1}(PF_{load})\right)}{\omega * V^2} \quad (40)$$

$$\sum_{i=0}^{N_L}(1 - R_i) * L_{min} * 2^i = -\frac{V^2}{\omega * P_{load}tan\left(cos^{-1}(PF_{load})\right)} \quad (41)$$

$$\sum_{i=0}^{N_C} R_i * 2^i = \frac{P_{load}tan\left(cos^{-1}(PF_{load})\right)}{C_{min}*\omega * V^2} \quad (42)$$

$$\sum_{i=0}^{N_L} \bar{R}_i * 2^i = -\frac{V^2}{L_{min}*\omega * P_{load}tan\left(cos^{-1}(PF_{load})\right)} \quad (43)$$

$$b_0 * 2^0 + b_1 * 2^1 + \cdots + b_n * 2^n = Decimal \quad (44)$$

5. RESULTS AND DISCUSSION

A plant underwent an evaluation in which a random selection of ten machines was chosen for assessment. Each of these machines comprised a variety of components, including induction heating systems, motors, vibrators, heating resistors, casting machines, molding machines, and more. Data collection took place at various random intervals, and this process was repeated multiple times. The initial set of collected data pertains to the first sample of the ten machines, which are referred to as devices. This data is presented in Table 4 and encompasses a range of electrical parameters linked to the load. These parameters encompass voltages V1, V2, and V3 across each phase and neutral, currents I1, I2, and I3 for each phase, power factors PF1, PF2, PF3, and PFt (the total power factor of the load), frequency F, real powers P1, P2, P3, and Pt (the total real power of the load), reactive powers Q1, Q2, Q3, and Qt (the total reactive power of the load), as well as apparent powers S1, S2, S3, and St (the total apparent power of the load). These parameters specifically relate to the load itself.

We conducted an initial analysis of the plant, revealing the absence of capacitive loads, which is a common occurrence in the industry due to their infrequent presence. As a result, the outcomes presented here are grounded in inductive loads. It's crucial to acknowledge that the same outcomes would hold true if capacitive loads were encountered.

Among the pivotal parameters identified during the analysis was the range of power per phase. We determined that the lowest power per phase ($P_{load,min}$) measured $189W$, while the highest power per phase ($P_{load,max}$) reached $56925W$. Utilizing these values, we computed the required minimum capacitance (C_{min}) at 2μF and the maximum capacitance (C_{max}) at 5478μF.

Table 4: Collected Data on Electrical Parameters and Load Characteristics from Ten Devices.

Name	Device_1	Device_2	Device_3	Device_4	Device_5	Device_6	Device_7	Device_8	Device_9	Device_10
V1	221.84	215.64	218.06	222.15	224.23	222.8	219.43	216.24	224.27	221.73
V2	226.57	215.57	215.11	225.01	228.2	229.94	210.74	214.03	212.45	225.59
V3	225.99	214.65	220	222.07	228.24	215.51	212.08	214.6	215	219.2
I1	83.59	202.72	35.31	125.57	222.99	133.47	186.98	102.23	44.28	169.59
I2	134.22	32.34	95.66	192.48	242.69	58.83	119.07	177.01	160.53	169.86
I3	107.11	121.68	224.98	192.44	75.88	201.21	88.13	131.02	219.67	188.06
PF1	0.66	0.66	0.8	0.68	0.69	0.76	0.67	0.78	0.63	0.68
PF2	0.72	0.66	0.69	0.65	0.77	0.76	0.64	0.67	0.7	0.78
PF3	0.79	0.64	0.69	0.71	0.71	0.76	0.65	0.63	0.66	0.64
PFt	0.73	0.65	0.7	0.68	0.73	0.76	0.66	0.69	0.67	0.7
F	50.05	50.74	50.69	50.36	50.22	50.7	50.25	50.03	50.56	50.38
P1	12238.78	28851.6	6159.76	18968.86	34500.72	22600.21	27489.44	17242.85	6256.33	25570.17
P2	21895.36	4601.21	14198.42	28151.45	42644.03	10280.8	16059.4	25383.25	23873.22	29888.6
P3	19122.57	16715.91	34151.96	30341.96	12296.38	32955.7	12148.9	17713.64	31171.17	26382.56
Pt	53256.71	50168.72	54510.14	77462.27	89441.13	65836.71	55697.74	60339.74	61300.72	81841.33
Q1	13931.17	32841.23	4619.82	20453.23	36191.23	19326.84	30458.35	13833.62	7712.11	27571.11
Q2	21103.91	5237.47	14894.13	32912.69	35336.06	8791.75	19280.69	28124.68	24355.55	23979.07
Q3	14840.73	20068.89	35825.38	30094.16	12195.96	28182.46	14203.63	21835.44	35481.56	31674.53
Qt	49875.81	58147.59	55339.33	83460.08	83723.25	56301.05	63942.67	63793.74	67549.22	83224.71
S1	18543.6	43714.54	7699.7	27895.38	50001.05	29737.12	41029.02	22106.22	9930.67	37603.19
S2	30410.23	6971.53	20577.42	43309.92	55381.86	13527.37	25092.81	37885.45	34104.6	38318.72
S3	24205.78	26118.61	49495.6	42735.15	17318.85	43362.76	18690.61	28116.89	47229.05	41222.75
St	72964.88	76798.72	77677.52	113868.29	122512.44	86627.25	84799.19	87809.6	91217.74	116723.42

Based on these computations, we established the necessity for 12 capacitors in the power factor correction system (NC=12). This configuration is essential for achieving the desired power factor correction in alignment with the given load parameters. However, it's noteworthy that the system has the capacity to accommodate a capacitance of up to 8,190μF if such a need arises.

Table 5 presents the necessary capacitance values for each phase (C1, C2, and C3) aimed at enhancing the power factor. These values are derived from the collected data showcased in Table 4. Additionally, the table illustrates the relay configuration status (R1, R2, and R3) required to achieve the intended capacity, along with the resulting capacity achieved (NC1, NC2, and NC3). The table also provides the corresponding reactive powers (QC1, QC2, QC3, and QCt), which collectively represent the total reactive power of the capacitors.

Table 5: Required Capacitance Values and Relay Configurations for Power Factor Enhancement.

Name	Device_1	Device_2	Device_3	Device_4	Device_5	Device_6	Device_7	Device_8	Device_9	Device_10
C1	900.17	2215.29	305.05	1309.8	2281.18	1222.2	2003.54	941.14	482.66	1771.61
C2	1307.3	353.52	1010.63	2054.44	2150.45	521.99	1375.03	1953.12	1698.63	1488.52
C3	924.04	1366.25	2324.04	1928.58	741.95	1904.83	1000.19	1508.32	2416.23	2082.53
R1	00011100 0010	01000101 0100	00001001 1001	00101000 1111	01000111 0101	00100110 0011	00111110 1010	00011101 0111	00001111 0001	00110111 0110
R2	00101000 1110	00001011 0001	00011111 1001	01000000 0011	01000011 0011	00010000 0101	00101011 0000	00111101 0001	00110101 0001	00101110 1000
R3	00011100 1110	00101010 1011	01001000 1010	00111100 0100	00010111 0011	00111011 1000	00011111 0100	00101111 0010	01001011 1000	01000001 0001
NC1	900	2216	306	1310	2282	1222	2004	942	482	1772
NC2	1308	354	1010	2054	2150	522	1376	1954	1698	1488
NC3	924	1366	2324	1928	742	1904	1000	1508	2416	2082
QC1	-13928.56	-32851.77	-4634.21	-20456.41	-36204.26	-19323.66	-30465.31	-13846.29	-7701.52	-27577.23
QC2	-21115.26	-5244.57	-14884.86	-32905.59	-35328.59	-8791.99	-19294.27	-28137.42	-24346.59	-23970.7
QC3	-14840.02	-20065.17	-35824.79	-30085.17	-12196.75	-28170.18	-14200.88	-21830.88	-35478.14	-31666.48
QCt	-49883.84	-58161.51	-55343.86	-83447.17	-83729.6	-56285.83	-63960.46	-63814.59	-67526.25	-83214.41

Upon implementing the capacitor configuration, the collected data is presented in Table 6. This dataset comprises the newly acquired values of reactive power, denoted as NQ1, NQ2, NQ3, and NQt, resulting from the integration of capacitors with the load. Additionally, the apparent power values after the integration of capacitors are indicated as NS1, NS2, NS3, and NSt. The updated power factors are represented by NPF1, NPF2, NPF3, and NPFt. Furthermore, the refreshed values of current consumption are specified as NI1, NI2, and NI3.

Table 6: Post-Integration Data for Reactive Power, Apparent Power, and Power Factors with Capacitors.

Name	Device_1	Device_2	Device_3	Device_4	Device_5	Device_6	Device_7	Device_8	Device_9	Device_10
NQ1	2.61	-10.54	-14.39	-3.18	-13.03	3.18	-6.96	-12.67	10.59	-6.12
NQ2	-11.35	-7.1	9.27	7.1	7.47	-0.24	-13.58	-12.74	8.96	8.37
NQ3	0.71	3.72	0.59	8.99	-0.79	12.28	2.75	4.56	3.42	8.05
NQt	-8.03	-13.92	-4.53	12.91	-6.35	15.22	-17.79	-20.85	22.97	10.3
AC1	99.981	99.968	99.689	99.984	99.964	99.984	99.977	99.908	99.863	99.978
AC2	99.946	99.865	99.938	99.978	99.979	99.997	99.93	99.955	99.963	99.965
AC3	99.995	99.981	99.998	99.97	99.994	99.956	99.981	99.979	99.99	99.975
ACt	99.984	99.976	99.992	99.985	99.992	99.973	99.972	99.967	99.966	99.988
NS1	12238.78	28851.6	6159.78	18968.86	34500.72	22600.21	27489.44	17242.85	6256.34	25570.17
NS2	21895.36	4601.22	14198.42	28151.45	42644.03	10280.8	16059.41	25383.25	23873.22	29888.6
NS3	19122.57	16715.91	34151.96	30341.96	12296.38	32955.7	12148.9	17713.64	31171.17	26382.56
NSt	53256.71	50168.72	54510.14	77462.27	89441.13	65836.71	55697.74	60339.74	61300.72	81841.33
NPF1	1	1	0.999997	1	1	1	1	1	0.999998	1
NPF2	1	0.999998	1	1	1	1	0.999999	1	1	1
NPF3	1	1	1	1	1	1	1	1	1	1
NPFt	1	1	1	1	1	1	1	1	1	1
NI1	55.17	133.8	28.25	85.39	153.86	101.44	125.28	79.74	27.9	115.32
NI2	96.64	21.34	66.01	125.11	186.87	44.71	76.2	118.6	112.37	132.49
NI3	84.62	77.88	155.24	136.63	53.87	152.92	57.28	82.54	144.98	120.36
PI1	56.439	56.437	35.991	53.757	52.392	42.237	55.108	39.159	60.3	53.761
PI2	48.158	56.458	52.383	57.751	40.711	42.242	59.045	55.108	51.001	39.161
PI3	37.585	59.035	52.388	49.592	49.599	42.24	57.757	60.313	56.441	59.039
PIt	47.052	57.334	50.868	53.761	46.909	42.239	56.907	53.127	54.842	51.288
Pr1	34	34	20	32	31	24	33	22	37	32
Pr2	28	34	31	35	23	24	36	33	30	22
Pr3	21	36	31	29	29	24	35	37	34	36
Prt	27.01	34.675	29.825	31.972	26.994	24	34.318	31.283	32.797	29.884

In our pursuit of a suitable accuracy metric (PFCP1, PFCP2, PFCP3, and PFCPt), our initial methodology centered around employing (45). This equation, designed to quantify accuracy as a percentage based on deviations from the desired power factor, showed promise. However, it revealed limitations in comprehensively capturing the intricacies inherent in our power factor correction process.

Given the distinct nature of our system, which involves manipulating reactive power to impact the power factor, the need for a more appropriate assessment metric was evident. This led to the introduction of an alternative metric (AC1, AC2, AC3, and ACt) denoted as (46), offering distinct advantages. (46) takes into account both the initial reactive power state and the absolute magnitude of reactive power change brought about by intentional adjustments. This formulation aligns closely with the physical components, including capacitors and inductors, that orchestrate these transformations.

The strength of (46) lies in its ability to precisely quantify the efficacy of power factor adjustments, while concurrently considering essential modifications in reactive power. This equation seamlessly harmonizes intricate dynamics, resulting in a more nuanced and insightful appraisal of system performance. By evaluating the proficiency of our system in managing the interaction between power factor adjustments and changes in reactive power, (46) provides a comprehensive measure of power factor correction accuracy that intimately reflects the real-world dynamics of our system. Additionally, to calculate the cumulative accuracy across devices for a specific time, we used (47), derived from (46), with "n" representing the number of devices.

Moving beyond accuracy, the effectiveness of our solution can be highlighted through the

metrics of power loss reduction and power consumption reduction. The percentages of power loss reduction (Pl1, Pl2, and Pl3) were calculated using (48), which can be expanded into (49) and (50). The overall power loss reduction (Plt) was computed using (51), derived from (48). Furthermore, to calculate the cumulative reduction in power loss across all devices for a specific time, we utilized (53), derived from (52), with "n" representing the number of devices. Similarly, the power usage reduction percentages (Pr1, Pr2, and Pr3) were determined using (54). The overall power usage reduction (Prt) was calculated using (55), with the total apparent power determined by (56). To calculate the cumulative reduction in power usage across all devices for a specific time, we employed (55), with the total apparent power determined by (57) and "n" representing the number of devices. These calculations offer valuable insights into the advancements achieved in terms of power loss and usage through the application of power factor correction measures.

$$PFCP_{(1,2,3,t)} = \left(1 - \left|\frac{NPFx-1}{1}\right|\right) * 100\% \quad (45)$$

$$AC_{(1,2,3,t)} = \frac{Q_{(1,2,3,t)}}{Q_{(1,2,3,t)}+|NQ_{(1,2,3,t)}|} * 100\% \quad (46)$$

$$tot_{AC} = \frac{\sum_{i=0}^{n} Q_{t,i}}{\sum_{i=0}^{n} Q_{t,i} - \sum_{i=0}^{n} NQ_{t,i}} * 100\% \quad (47)$$

$$Pl_{(1,2,3)} = \frac{Pj_{(1,2,3),old} - Pj_{(1,2,3),new}}{P_{j(1,2,3),old}} * 100\% \quad (48)$$

$$Pl_{(1,2,3)} = \frac{R_{(1,2,3)} * I^2_{(1,2,3),old} - R_{(1,2,3)} * I^2_{(1,2,3),new}}{R_{(1,2,3)} * I^2_{(1,2,3),old}} * 100\% (49)$$

$$Pl_{(1,2,3)} = \frac{I^2_{(1,2,3),old} - I^2_{(1,2,3),new}}{I^2_{(1,2,3),old}} * 100\% \quad (50)$$

$$Plt = \frac{\sum_{i=0}^{3} Pj_{i,old} - \sum_{i=0}^{3} Pj_{i,new}}{\sum_{i=0}^{3} P_{j,i,old}} * 100\% \quad (51)$$

$$Plt = \frac{\sum_{i=0}^{3} I^2_{i,old} - \sum_{i=0}^{3} I^2_{i,new}}{\sum_{i=0}^{3} I^2_{i,old}} * 100\% \quad (52)$$

$$tot_{Plt} = \frac{\sum_{i=0}^{n}\left(\sum_{j=0}^{3} I^2_{i,j,old} - \sum_{j=0}^{3} I^2_{i,j,new}\right)}{\sum_{i=0}^{n}\left(\sum_{j=0}^{3} I^2_{i,j,old}\right)} * 100\% \quad (53)$$

$$Pr_{(1,2,3)} = \frac{S_{(1,2,3),old} - S_{(1,2,3),new}}{S_{(1,2,3),old}} * 100\% \quad (54)$$

$$Prt = \frac{St_{old} - St_{new}}{St_{old}} * 100\% \quad (55)$$

$$St_{(old,new)} = \sqrt{Pt_{(old,new)}{}^2 + Qt_{(old,new)}{}^2} (56)$$

$$St_{(old,new)} = \sqrt{\left(\sum_{i=0}^{n} Pt_{i,(old,new)}\right)^2 + \left(\sum_{i=0}^{n} Qt_{i,(old,new)}\right)^2} (57)$$

In addition to the data presented in Tables 4, 5, and 6, which encapsulate the information gathered from the initial set of ten devices, our research expands to encompass successive data collection phases. This ongoing data collection process produces new datasets that mirror the structure of Tables 4, 5, and 6. As time progresses, each new dataset provides further insights into the behavior of the devices under varying conditions.

Upon meticulous analysis of the data in Tables 4, 5, and 6 and their counterparts from subsequent collection phases, several crucial observations arise concerning the inherent non-linearity of the loads. Each individual phase distinctly exhibits its own unique current and power factor values ($PF_1 \neq PF_2 \neq PF_3$). Furthermore, the non-linear characteristics of the loads exhibit fluctuations over time ($PF_{1,t0} \neq PF_{1,t1} \neq PF_{1,t2} \cdots ; PF_{2,t0} \neq PF_{2,t1} \neq PF_{2,t2} \cdots ; PF_{3,t0} \neq PF_{3,t1} \neq PF_{3,t2} \cdots$). This underscores the importance of considering adaptable capacitance solutions tailored to the complexities of the system. Even when opting for variable capacitance solutions, maintaining independent control over the capacitance of each phase remains paramount.

Given the substantial power consumption and the dynamic nature of load behavior, strategically distributing the capacitor banks across each individual load is advisable. This allocation strategy helps minimize the necessity for frequent switching relays due to load variations. Additionally, it is essential to note that deploying a substantial capacitor bank could lead to increased current demand and the generation of harmonics, phenomena particularly relevant in this context.

The introduction of power factor correction yields notable enhancements in power factor within this system, with most values converging toward the desired optimal value of 1.0. This corrective measure not only reduces apparent power, resulting in tangible cost savings, but also diminishes current draw, subsequently curbing power loss. Furthermore, the resulting capacitance values after implementing these corrections closely align with the intended capacitance levels.

It is pertinent to highlight that the degree of deviation from the power factor of 1.0 corresponds with the potential for reducing power consumption

Journal of Theoretical and Applied Information Technology
15th January 2024. Vol.102. No 1

ISSN: 1992-8645 www.jatit.org E-ISSN: 1817-3195

and mitigating power loss within the system. As such, lower power factor values indicate a greater potential for achieving these favorable outcomes.

Demonstrating the effectiveness of our approach, we randomly selected 30 samples from the pre-collected data. In Figure 18, we highlight the accuracy of our method across various time intervals for each device. ACt_1 through ACt_30 represent the overall accuracy of specific devices at certain time points. This figure vividly illustrates our method's consistent achievement of accuracy surpassing 98.889% for any device within the given time frame.

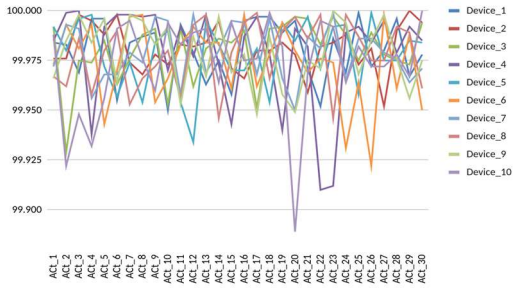

Figure 18: Accuracy Trends of Methodology Across Various Time Intervals for Individual Devices.

Moving on to Figure 19, we present the cumulative accuracy across devices for specific time intervals. Notably, our method consistently attains a total accuracy exceeding 99.988% in every time step.

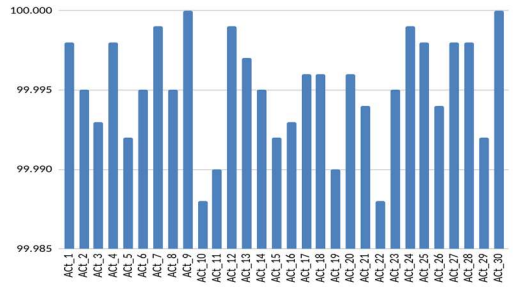

Figure 19: Cumulative Accuracy Across Devices for Specific Time Intervals.

Figure 20 captures the power loss reduction achieved by our approach for individual devices across different time intervals. Plt_1 through Plt_30 denote the total power loss reduction percentage for specific devices at certain times. It is evident that our method consistently achieves power loss reduction surpassing 37.858% for any device within the specified time period.

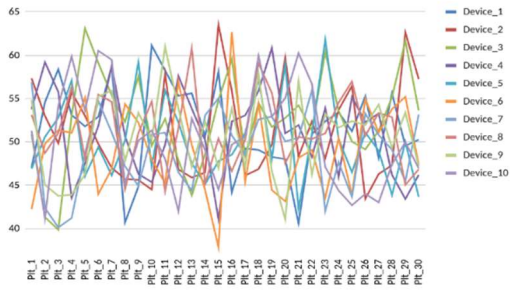

Figure 20: Total Power Loss Reduction Percentage for Individual Devices Across Different Time Intervals.

In Figure 21, we portray the cumulative power loss reduction across devices for a specific time. Impressively, our method sustains a substantial overall reduction in power loss, exceeding 48.078% in each time step.

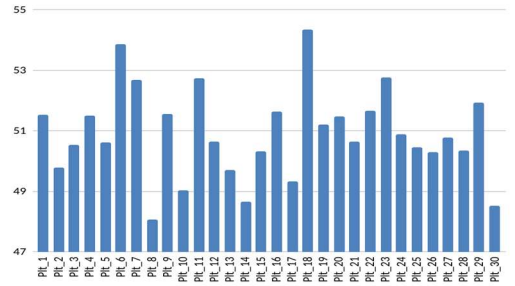

Figure 21: Cumulative Power Loss Reduction Across Devices for Specific Time Intervals.

Figure 22 delves into the trends of power usage reduction for different devices and time intervals. Prt_1 through Prt_20 represent the total power usage reduction percentages for specific devices during designated time periods. Here, we observe our method's consistent accomplishment of power usage reduction surpassing 21.116% for any device at a given time.

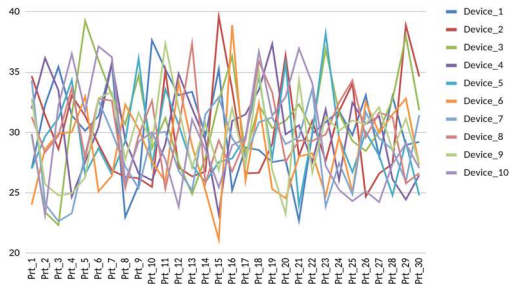

Figure 22: Power Usage Reduction Percentages for Individual Devices Over Time.

Likewise, Figure 23 presents the cumulative power usage reduction across devices for a specific time. The data reaffirms our method's

consistent achievement of total reduction in power usage, surpassing 27.862% for every time step.

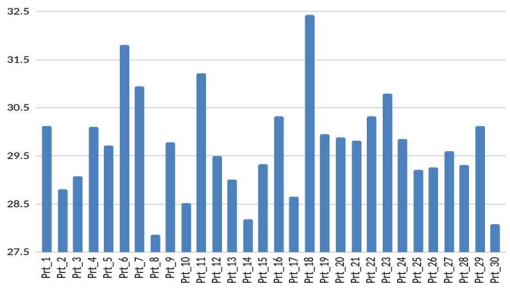

Figure 23: Cumulative Power Usage Reduction Across Devices for Specific Time Intervals.

In summary, the comprehensive data presented in the figures effectively bolsters our methodology's accuracy, power loss reduction capabilities, and its notable impact in optimizing power usage.

6. CONCLUSION

In summary, our research has effectively addressed the pivotal challenge of load unbalances in three-phase systems within Industry 4.0 environments. By implementing a dynamic and real-time power factor correction methodology, we have successfully demonstrated a substantial enhancement in energy efficiency and operational sustainability. This achievement represents a significant stride in the evolution of smart manufacturing processes.

Our approach, which hinges on the strategic integration of Power Monitoring and Control Units (PMCU), has proven to be a game-changer in the realm of industrial power distribution. The real-time adjustments of capacitors and inductors facilitated by our system have ensured that each load's power factor consistently approaches unity, optimizing energy utilization and reducing wastage.

The implications of this study are manifold. On a practical level, the introduction of our methodology in industrial settings could lead to decreased energy consumption, escalated cost savings, and reduced strain on equipment. In a broader context, our work contributes to the ongoing transformation towards enhanced industrial efficiency, sustainability, and economic viability.

However, our journey does not end here. The potential for further research and development in this field is vast. Future studies could explore the scalability of this system across various industrial sectors, its integration with renewable energy sources, and the long-term impacts on industrial energy management. Additionally, there's room to investigate the interplay between our methodology and other Industry 4.0 technologies, such as machine learning algorithms and advanced data analytics, to further refine and optimize power distribution systems.

In closing, our work not only provides a robust solution to a longstanding issue in industrial power systems but also lays the groundwork for more innovative, efficient, and intelligent power management strategies in the era of Industry 4.0.

REFERENCES:

[1] H. Lasi, P. Fettke, H. G. Kemper, T. Feld, and M. Hoffmann, "Industry 4.0," *Bus. Inf. Syst. Eng. 2014 64*, vol. 6, no. 4, pp. 239–242, Jun. 2014, doi: 10.1007/S12599-014-0334-4.

[2] S. Schneider, "THE INDUSTRIAL INTERNET OF THINGS (IIoT)," *Internet Things Data Anal. Handb.*, pp. 41–81, Feb. 2017, doi: 10.1002/9781119173601.CH3.

[3] H. Boyes, B. Hallaq, J. Cunningham, and T. Watson, "The industrial internet of things (IIoT): An analysis framework," *Comput. Ind.*, vol. 101, pp. 1–12, Oct. 2018, doi: 10.1016/J.COMPIND.2018.04.015.

[4] E. G. Popkova, Y. V. Ragulina, and A. V. Bogoviz, *Industry 4.0: Industrial Revolution of the 21st Century*, vol. 1100 AISC. Cham: Springer International Publishing, 2020.

[5] L. Da Xu, E. L. Xu, and L. Li, "Industry 4.0: state of the art and future trends," *https://doi.org/10.1080/00207543.2018.1444806*, vol. 56, no. 8, pp. 2941–2962, 2018, doi: 10.1080/00207543.2018.1444806.

[6] O. García, J. A. Cobos, R. Prieto, P. Alou, and J. Uceda, "Single phase power factor correction: A survey," *IEEE Trans. Power Electron.*, vol. 18, no. 3, pp. 749–755, May 2003, doi: 10.1109/TPEL.2003.810856.

[7] Z. Pan, F. Z. Peng, and S. Wang, "Power factor correction using a series active filter," *IEEE Trans. Power Electron.*, vol. 20, no. 1, pp. 148–153, Jan. 2005, doi: 10.1109/TPEL.2004.839819.

[8] F. Zheng and W. Zhang, "Long term effect of power factor correction on the industrial load: A case study," *2017 Australas. Univ. Power Eng. Conf. AUPEC 2017*, vol. 2017-November, pp. 1–5, Feb. 2018, doi: 10.1109/AUPEC.2017.8282382.

[9] M. A. Graña-López, A. García-Diez, A.

Filgueira-Vizoso, J. Chouza-Gestoso, and A. Masdías-Bonome, "Study of the sustainability of electrical power systems: Analysis of the causes that generate reactive power," *Sustain.*, vol. 11, no. 24, p. 7202, Dec. 2019, doi: 10.3390/SU11247202.

[10] H. Kirkham, A. Emanuel, M. Albu, and D. Laverty, "Resolving the reactive power question," *I2MTC 2019 - 2019 IEEE Int. Instrum. Meas. Technol. Conf. Proc.*, vol. 2019-May, May 2019, doi: 10.1109/I2MTC.2019.8826915.

[11] Y. Zerguit, Y. Hammoudi, I. Idrissi, and M. Derrhi, "A RELAY-BASED AUTOMATIC BALANCING SYSTEM FOR THREE-PHASE LOADS IN INDUSTRY 4.0," *J. Theor. Appl. Inf. Technol.*, vol. 101, no. 5, pp. 2012–2026, Mar. 2023.

[12] M. Grari *et al.*, "Using IoT and ML for Forest Fire Detection, Monitoring, and Prediction: a Literature Review," *J. Theor. Appl. Inf. Technol.*, vol. 100, 2022.

[13] M. Yandouzi *et al.*, "Review on forest fires detection and prediction using deep learning and drones," *J. Theor. Appl. Inf. Technol.*, vol. 100, no. 12, pp. 4565–4576, 2022.

[14] I. Idrissi, M. Azizi, and O. Moussaoui, "A Stratified IoT Deep Learning based Intrusion Detection System," in *2022 2nd International Conference on Innovative Research in Applied Science, Engineering and Technology (IRASET)*, Mar. 2022, pp. 1–8, doi: 10.1109/IRASET52964.2022.9738045.

[15] Y. Hammoudi, I. Idrissi, M. Boukabous, Y. Zerguit, and H. Bouali, "Review on maintenance of photovoltaic systems based on deep learning and internet of things," *Indones. J. Electr. Eng. Comput. Sci.*, vol. 26, no. 2, pp. 1060–1072, May 2022, doi: 10.11591/IJEECS.V26.I2.PP1060-1072.

[16] "What is Three Phase System? Definition & Types - Circuit Globe." https://circuitglobe.com/three-phase-system.html (accessed Nov. 21, 2021).

[17] J. B. V Subrahmanyam and E. Engg, "LOAD FLOW SOLUTION OF UNBALANCED RADIAL DISTRIBUTION SYSTEMS," *J. Theor. Appl. Inf. Technol.*, 2009.

[18] C. K. Chang, S. T. Cheng, and B. K. Boyanapalli, "Three-Phase Unbalance Improvement for Distribution Systems Based on the Particle Swarm Current Injection Algorithm," *Energies 2022, Vol. 15, Page 3460*, vol. 15, no. 9, p. 3460, May 2022, doi: 10.3390/EN15093460.

[19] "Three Phase Balanced vs unbalanced system / load - TheElectricalGuy." https://www.theelectricalguy.in/tutorials/three-phase-balanced-vs-unbalanced-system-load/ (accessed Nov. 21, 2021).

[20] C. M. Coman, A. Florescu, and C. D. Oancea, "Improving the Efficiency and Sustainability of Power Systems Using Distributed Power Factor Correction Methods," *Sustain. 2020, Vol. 12, Page 3134*, vol. 12, no. 8, p. 3134, Apr. 2020, doi: 10.3390/SU12083134.

[21] B. M. Rija, M. K. Hussain, and A. M. Vural, "Microcontroller Based Automatic Power Factor Correction for Single-Phase Lagging and Leading Loads," *Eng. Technol. Appl. Sci. Res.*, vol. 10, no. 6, pp. 6515–6520, Dec. 2020, doi: 10.48084/etasr.3916.

[22] K. Alam, L. Sharma, and N. Chopra, "Power Factor Correction for Single-Phase Domestic Loads Using Microcontroller and Triac," *Lect. Notes Networks Syst.*, vol. 151, pp. 91–103, 2021, doi: 10.1007/978-981-15-8218-9_8/COVER.